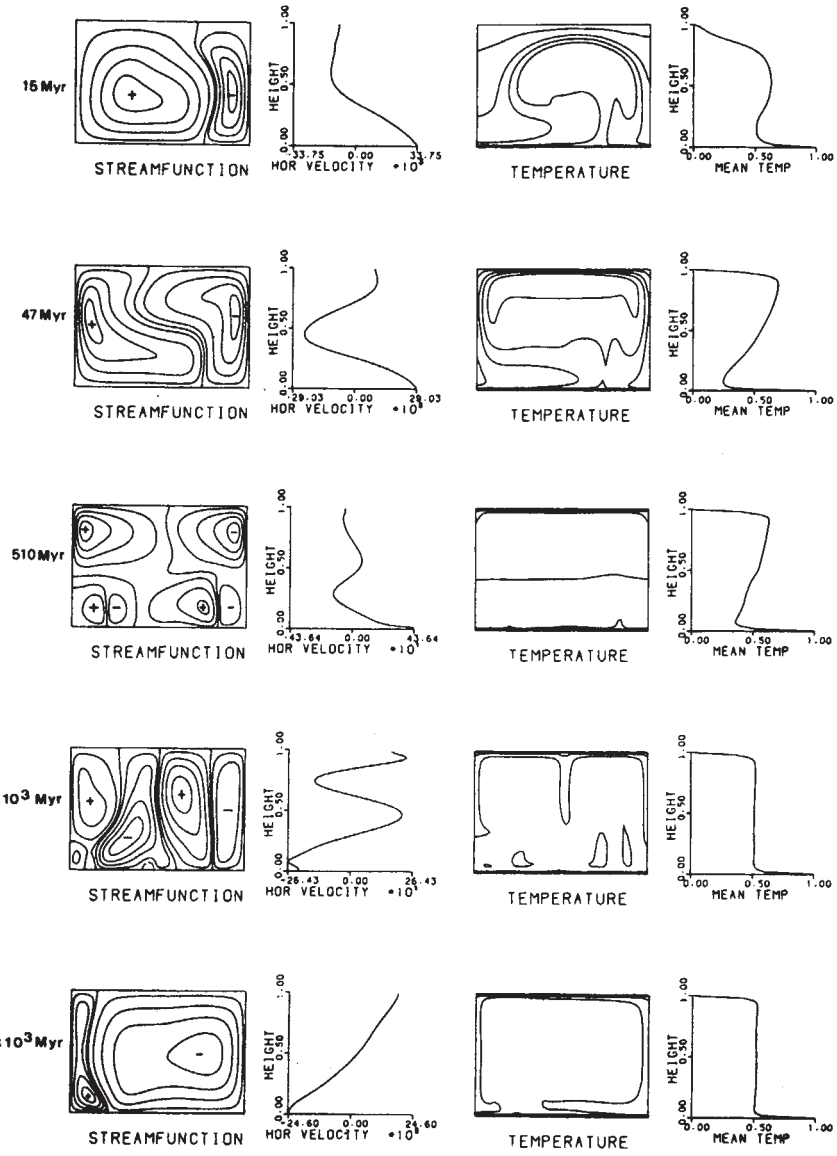


**Fig. 2** Time evolution of a model of mantle convection with $Ra = 10^7$ (see Fig. 1 legend). Note the presence of a transient period of double-layer convection, evidenced by the streamfunction (closed streamlines of the fluid flow) at 510 Myr.

value better. Thus, this mechanism provides another means, besides chemical density changes, of enforcing stratification of convective layers, though only in a transient manner. While these results are possibly significant for models of the Earth's evolution; they should be verified on higher spatial resolution grids, as well as with different numerical methods. The assumed initial conditions are critical for inversion and thus require further investigation.

This work was partially supported by NASA.

Received 21 November 1983; accepted 14 February 1984.

1. Schubert, G. *A. Rev. Earth planet. Sci.* **7**, 289–342 (1979).
2. Davies, G. F. *Geophys. J. R. astr. Soc.* **49**, 459–486 (1977).
3. Elsasser, W. M., Olson, P. & Marsh, B. D. *J. geophys. Res.* **84**, 147–155 (1979).
4. Jeanloz, R. & Richter, F. M. *J. geophys. Res.* **84**, 5497–5504 (1979).
5. Olson, P. *J. geophys. Res.* **86**, 4881–4890 (1981).
6. Richter, F. M. & McKenzie, D. P. *J. geophys. Res.* **86**, 6133–6142 (1981).
7. Schubert, G. & Spohn, T. *Geophys. Res. Lett.* **8**, 951–954 (1981).
8. Fowler, A. C. *Geophys. Res. Lett.* **9**, 816–819 (1982).
9. Kenyon, P. M. & Turcotte, D. L. *J. geophys. Res.* (submitted).
10. Spohn, T. & Schubert, G. *J. geophys. Res.* **87**, 4682–4696 (1982).
11. Hofmann, A. W., White, W. M. & Whitford, D. J. *Carnegie Instn Wash. Yb.* **77**, 548–562 (1978).
12. DePaolo, D. J. *Nature* **291**, 193–196 (1981).
13. Jacobsen, S. B. & Wasserburg, G. J. *Tectonophysics* **75**, 163–179 (1981).
14. Allegre, C. J. *Tectonophysics* **81**, 109–132 (1982).
15. Christensen, U. *Geophys. J. R. astr. Soc.* **68**, 487–497 (1982).
16. Olson, P. & Yuen, D. A. *J. geophys. Res.* **87**, 3993–4002 (1982).
17. Richter, F. M. & McKenzie, D. P. *J. geophys. Res.* **86**, 6133–6142 (1981).
18. Peltier, W. R. *A. Rev. Earth planet. Sci.* **9**, 199–225 (1981).
19. Andrews, D. J. *J. geophys. Res.* **77**, 6470–6481 (1972).
20. Young, R. E. *J. Fluid Mech.* **63**, 695–721 (1974).
21. McKenzie, D. P., Roberts, J. M. & Weiss, N. O. *J. Fluid Mech.* **62**, 465–538 (1974).
22. Schubert, G. & Young, R. E. *Tectonophysics* **35**, 201–214 (1976).
23. Daly, S. F. *Geophys. J. R. astr. Soc.* **61**, 519–547 (1980).
24. Arkani-Hamed, J., Toksoz, M. N. & Hsui, A. T. *Tectonophysics* **75**, 19–30 (1981).
25. Houseman, G. & McKenzie, D. P. *Geophys. J. R. astr. Soc.* **68**, 133–164 (1982).
26. Boss, A. P. & Sacks, I. S. *Carnegie Instn Wash. Yb.* **81**, 543–550 (1982).
27. Lux, R. A. & Sacks, I. S. *Carnegie Instn Wash. Yb.* **79**, 512–520 (1980).
28. Torrance, K. E. & Turcotte, D. L. *J. Fluid Mech.* **47**, 113–125 (1971).
29. Schubert, G., Cassen, P. & Young, R. E. *Phys. Earth planet. Interiors* **20**, 194–208 (1979).
30. Stevenson, D. J. *Science* **214**, 611–619 (1981).
31. Basaltic Volcanism Study Project. *Basaltic Volcanism on the Terrestrial Planets*, 1163 (LPI, Houston, Texas, 1981).

# Stagnant layers at the bottom of convecting magma chambers

**Claude Jaupart, Geneviève Brandeis & Claude J. Allègre**

Laboratoire de Géochimie et Cosmochimie, Institut de Physique du Globe et Département des Sciences de la Terre, Université Paris 6 et 7, 4 place Jussieu, 75230 Paris Cedex 05, France

**The evolution and crystallization of igneous complexes has received much attention from petrologists[1–3] and more recently from physicists[4–10]. Current models emphasize the role of compositional effects. We present here a different viewpoint. Because compositional effects are due to crystallization, they depend on the thermal structure and regime of cold boundary layers in convecting magma chambers, particularly of the bottom layer where the thickest rock sequences form. We have studied purely thermal convection in a large aspect ratio magma chamber which is cooled through both its upper and lower boundaries.**

**We made laboratory fluid dynamical experiments in turbulent and transient conditions and show that a stagnant layer develops at the bottom, isolated from the convective part of the chamber. The essential features of this layer are that it is not affected by mixing and that a significant thermal gradient is maintained across it. These imply peculiar crystallization conditions.**

We have studied the sudden cooling of an initially hot and isothermal layer of fluid. The fluid is placed in a Plexiglass tank of 25×25 cm horizontal dimensions and 10 cm height. The tank walls are 2 cm thick to minimize lateral heat losses. Fixed temperature boundary conditions are achieved using two 3-cm thick copper plates at the upper and lower surfaces, through which thermostated water circulates. At the beginning of the experiment, temperature is uniform in the fluid and in both copper plates at a value $T_0$. At time $t=0$, the copper plates are switched to a cold water bath. They are cooled rapidly, reaching 90% of their final temperature in about 2.5 min. Temperature is maintained constant at a lower value $T_0-\Delta T$ to within 0.1 °C after 6 min. These conditions approximate those of instantaneous cooling.

In the standard Boussinesq approximation and for the fixed temperature boundary conditions of interest here, two non-dimensional parameters characterize the experiments[11,12]: Rayleigh number $\mathrm{Ra}=(g\alpha\Delta T d^3)/\kappa\nu$ and Prandtl number $\mathrm{Pr}=\nu/\kappa$, where $d$ is the thickness of the layer, $g$ the acceleration due to gravity, $\alpha$ the coefficient of thermal expansion, $\kappa$ thermal diffusivity and $\nu$ kinematic viscosity. We assume that viscosity is constant (in our experiments, it never varies by more than 30%). In natural systems, viscosity depends strongly on temperature. For such fluids, theoretical calculations as well as laboratory experiments have shown that convective flows are limited to regions where viscosity variations are small and resemble the uniform viscosity flows[13–15]. We have investigated the constant viscosity problem as it is a prerequisite to a proper understanding of the more complex variable viscosity problem. We do not include compositional effects which result from crystallization and therefore depend on the cooling regime.

The physical properties of basaltic liquids[16–19] indicate that representative Prandtl numbers exceed 4,000. For a temperature difference of 50 °C and a chamber height of 1 km, the Rayleigh number is extremely large ($10^{16}$). We used silicone oil with kinematic viscosities ranging over $10^2$–$10^3$ mm$^2$ s$^{-1}$. For those, Pr ranges from 800 to 8,000. The proper scaling of our experiments can be made using the analysis of Kraichnan for high Prandtl number fluids[12]. The range of Rayleigh numbers investigated is $10^6$–$10^8$ and molecular viscosity dominates the whole flow structure. This is always the case in boundary layers, whatever the Rayleigh number value, and it is this that we have investigated.

Several types of observations were made. Shadowgraph pictures allow the visualization of the whole temperature structure (see ref. 17). To obtain a more detailed picture of convection, we also used differential interferometry[20] with a 4-cm-wide laser beam. This gives a picture of the iso-gradient temperature lines to an accuracy of about 0.01 °C cm$^{-1}$. Finally, we placed a series of 11 thin (0.2 mm diameter) platinum wires stretched horizontally across the fluid. These allow the measurement of the mean horizontal temperature to an accuracy of about 0.2 °C, or typically 1% of the overall temperature difference.

We have run more than 15 experiments with different oils and varying temperature differences. All showed the same effects, which we now describe for one experiment run with $\Delta T=22.2$ °C and $\mathrm{Ra}=5.9\times10^6$. Convective instability starts at about 2 min (Fig. 1*a*), when a local Rayleigh number based on the thermal boundary layer thickness exceeds a value of about 1,600 in agreement with other studies[21]. The boundary layer breakdown occurs in the form of thermals or, more accurately, 'starting plumes'[22]. These take about 1 min to reach the lower parts of the fluid (Fig. 1*b*). In this initial stage, they almost penetrate to the lower surface. With time the thermals become

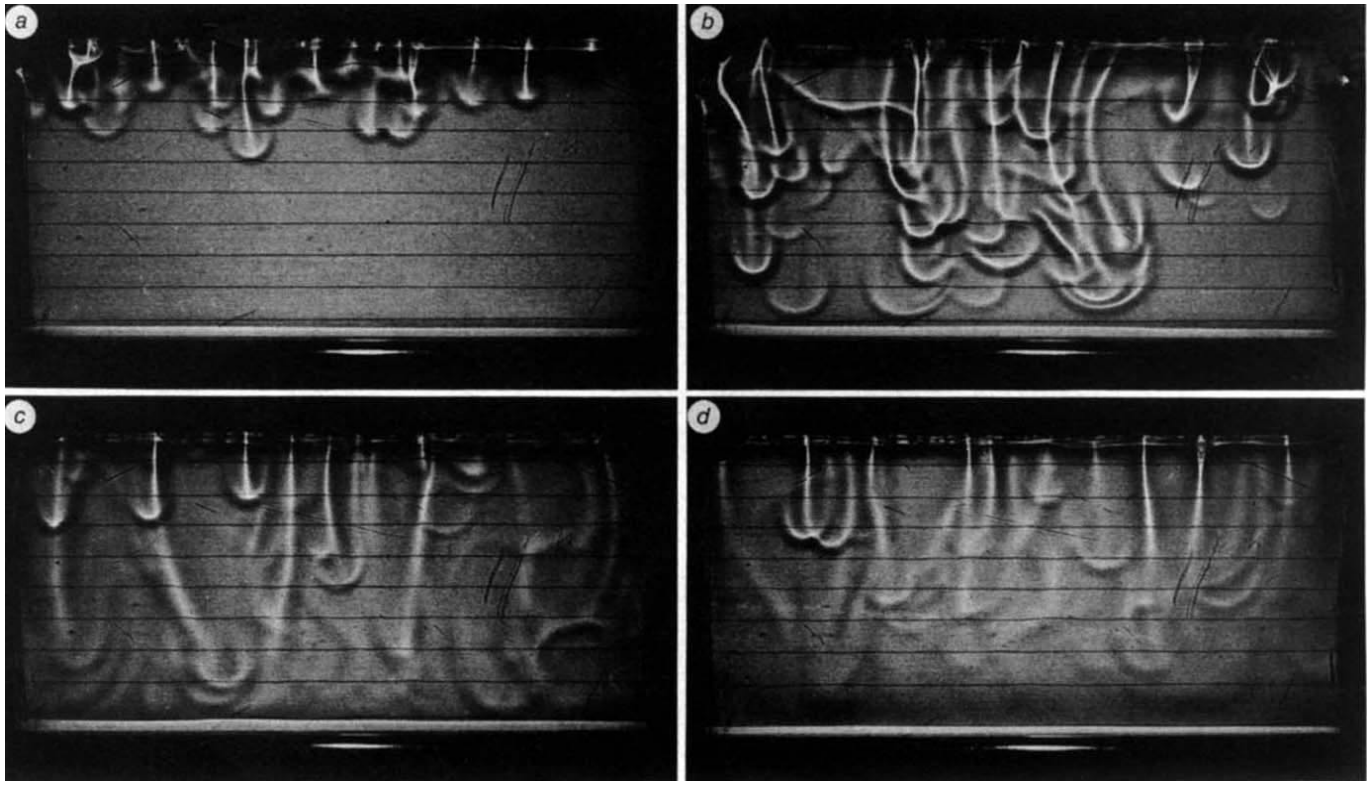


**Fig. 1** Time-sequence of the development of convection for the experiment discussed in the text. The lower boundary layer is barely detectable because of light refraction (the wire which is seen at the very bottom lies at 1 cm above the lower surface). The right end of the upper boundary layer goes unstable slightly later than the left end because cooling is not perfectly uniform initially. The effect is not large, as witnessed by the small difference in onset time. *a*, Convection starts: thermals are generated in the upper boundary layer. *b*, The convective thermals or 'starting plumes' reach the bottom. *c*, Fully developed convection (time 4′30″). *d*, Convection in a late stage (time 13′30″). Compare with *c* and *b*. The grey area at the very bottom is not penetrated by thermals: this is the stagnant layer.

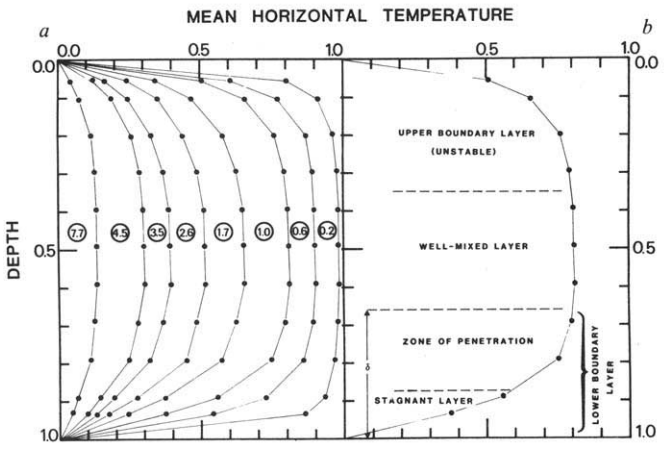


**Fig. 2** *a*, Vertical profiles of the mean horizontal temperature as time increases. Numbers along the curves indicate the non-dimensional time, defined as $(d^2 t/\kappa)$, in units of $10^{-2}$. Real times are, in minutes: 3, 9, 15, 27, 40, 55 and 90. Steady-state conditions are reached in about 4 h for this experiment. *b*, Schematic structure of convection for the profile at 1.0 (15 min) from both the temperature data and the photographs.

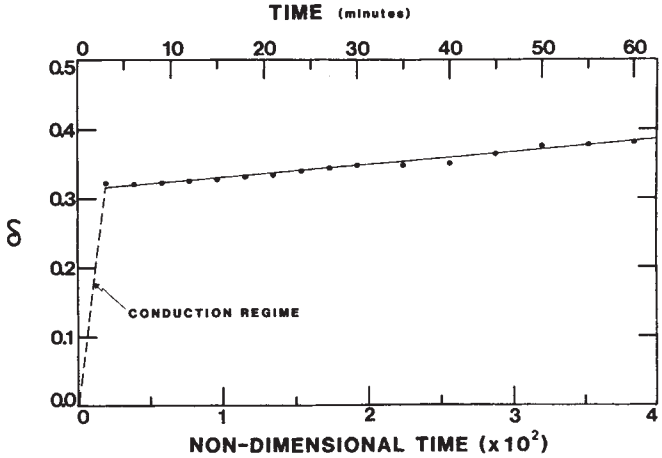


**Fig. 3** Evolution of $\delta$, the lower boundary layer thickness (in units of $d$, the total layer thickness). Note the initial period of fast growth when there is no convection. Within experimental error, the data can be fitted with a straight line.

slower and do not reach the bottom (compare Figs 1*b*, *d*): a stagnant layer of significant thickness has formed. The thermals travel in the fluid with an approximately constant velocity until they are strongly decelerated and then stop at the top of the stagnant layer. The zone of deceleration corresponds to that of penetration of the stable temperature gradient at the base of the tank.

The general structure of convection is described in Fig. 2. At the top there is an unstable boundary layer where thermals are generated. In the middle parts of the fluid the mean horizontal temperature is approximately constant (within experimental accuracy). This defines a well-mixed layer. Below this, the lower thermal boundary layer is made of two parts: a zone of penetration where thermals decelerate and a stagnant layer where there is no convection. Note that the temperature gradient is large in the stagnant layer. This is associated with a density increase which does not allow penetration.

The profiles of Fig. 2 indicate that the thickness of the well-mixed layer decreases slowly with time as cooling proceeds and convection becomes more sluggish. This can be shown by the growth of the lower boundary layer. Its thickness was determined by fitting a second-degree polynomial to the temperature data and then calculating the height at which temperature has a zero vertical gradient. Figure 3 shows that this thickness evolves very slowly with time after an initial period of formation, which is simply the conduction stage before the convective thermals reach the bottom. The evolution of the stagnant layer is similar. After an initial episode of fast growth, its thickness stabilizes and increases almost imperceptibly.

To confirm the existence of the stagnant layer, we used differential interferometry. Because in the case of cooling the light rays are refracted into the stagnant layer, no clear and simple picture can be obtained. We therefore performed the reverse experiment and suddenly heated an initially cold fluid layer. A stagnant layer was observed at the top, which is shown in Fig. 4 as a convective thermal approaches. Note that it does not penetrate the layer and is dissipated by conduction and by other incoming thermals. In the cooling experiment, the lower boundary layer is colder and therefore more viscous than the rest of the fluid, which impedes the penetration of thermals. However, the formation of the stagnant layer is not a result of viscosity increase, as evidenced by the heating experiment.

The existence of a stagnant layer is a universal feature of all our experiments. This layer grows by the addition of cold fluid

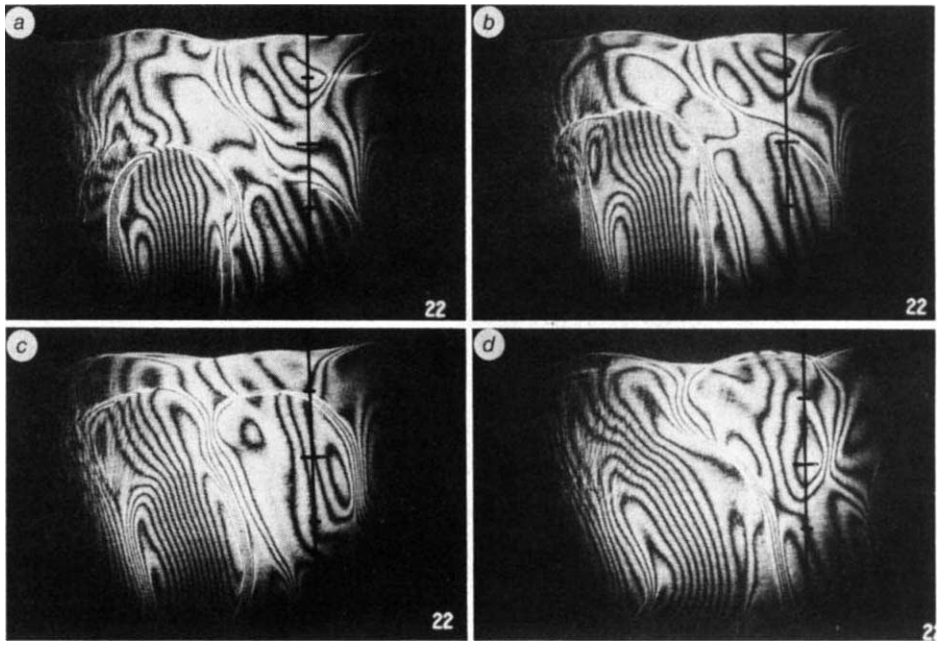


**Fig. 4** Differential interferometry for the reverse experiment: a cold layer is heated suddenly from both upper and lower boundaries. $\Delta T$ was 10.5 °C and Ra $8.5 \times 10^6$. The photographs were taken after 45 min when the temperature difference between the well-mixed layer and both copper plates was 3.9 °C. Photographs are taken at 20-s intervals. The marks on the right-hand side are 1 cm apart. The dark region at the top with the wavy interface is the stagnant layer. There is an incoming thermal in *a*. Note the slight distortion of the interface ahead of the thermal cap. The patterns are complex because the laser beam crosses the whole fluid and averages the effect of the thermal with that of the background.

coming from the top. The basic physical principle is simple and has been illustrated in other types of experiments[23,24]: cold fluid is stable and nothing will make it rise. Cooling through side-walls would enhance the effect. Our results are therefore of general applicability and do not depend on our particular set of initial conditions (for example, whether or not the temperatures of the upper and lower surfaces are lowered by the same amount). The thickness of the stagnant layer may change, but not the fact that it exists. What is more important and new is that the stagnant layer stabilizes rapidly at some thickness. This shows that penetration is also stabilized. The convective system thus evolves towards a stable spatial configuration which then changes slowly. The physics of this are complex, involving transient convection and penetration in a non-uniform environment. The physical and mathematical treatment of the temperature data allow some further developments and scaling laws. These will be made in a more extensive study.

There is some observational support for the existence of a stagnant layer. Donaldson[25] suggested that crystals formed in a quiet environment in the Rhum intrusion. Similarly, Jackson[1] argued that textures and structures in the Ultramafic Zone of the Stillwater Complex indicate that magma was stagnant. Our experiments imply peculiar crystallization conditions at the bottom of magma chambers. There, crystals would not be affected by convective mixing phenomena. Furthermore, crystallization would occur with a rather high heat flux imposed from the top (Fig. 2). This represents highly unstable conditions for crystal nucleation and growth and probably leads to cyclic crystallization sequences on the scale of a few centimetres[26,27]. More generally, the conditions clearly differ from those in a large reservoir as the stagnant layer is of smaller thickness. In particular, crystallization is slower because country rocks must evacuate both the latent heat of crystallization and the imposed heat flux.

The main limitation of our experiments is the absence of compositional effects. Such effects develop in crystallizing regions where there is a high density of crystals. Because magmas are viscous, the associated density instabilities are not instantaneous. What must be ascertained is whether these instabilities develop before or after the formation of the stagnant layer. If they develop after, they would lead to the destruction of the stagnant layer, which would then form again. This process could repeat itself in a quasi-periodic manner.

Our aim has been to investigate one of the simplest fluid dynamical experiments of relevance to the study of magma chamber processes. In conclusion, the stagnant layer isolates the crystallizing region below from the effects of convective mixing. It represents a smaller volume of magma in which compositional gradients may be set up and destroyed. This offers a physical alternative to the reinjection hypothesis to explain relatively rapid cyclic chemical evolution within large magma chambers.

This study was supported by PIRPSEV and by INAG (ATP Geodynamique 2). We thank P. Bergé for advice, M. Girard, L. P. Ricard and A. Lecomte for help in the laboratory, and Y. Bottinga, H. Huppert, B. D. Marsh, S. A. Morse and H. S. Yoder for thoughtful comments. This is IPGP Contribution No. 724.

Received 6 October 1983; accepted 5 January 1984.

1. Jackson, E. D. *U.S. Geol. Surv. Prof. Pap.* 358 (1961).
2. Wager, L. R. & Brown, G. M. *Layered Igneous Rocks* (Oliver & Boyd, Edinburgh, 1967).
3. Morse, S. A. *J. Petrol.* **20,** 555–624 (1979).
4. McBirney, A. R. & Noyes, R. M. *J. Petrol.* **20,** 487–554 (1979).
5. Chen, C. F. & Turner, J. S. *J. geophys. Res.* **85,** 2573–2593 (1980).
6. Turner, J. S. *Nature* **285,** 213–215 (1980).
7. Irvine, T. N. in *Physics of Magmatic Processes* (ed. Hargraves, R. B.) 325–383 (Princeton University Press, 1980).
8. Huppert, H. E. & Sparks, R. S. J. *Nature* **286,** 46–58 (1980); *Contr. Miner. Petrol.* **75,** 279–289 (1980).
9. Huppert, H. E. & Turner, J. S. *Earth planet. Sci. Lett.* **54,** 144–152 (1981).
10. Usselman, T. M. & Hodge, D. S. *J. Volcanol. geotherm. Res.* **4,** 265–281 (1978).
11. Busse, F. H. *Rep. Prog. Phys.* **41,** 1930–1967 (1978).
12. Kraichnan, R. H. *Phys. Fluids* **5,** 1374–1389 (1962).
13. Jaupart, C. thesis, Massachusetts Instit. Technol. (1981).
14. White, D. thesis, Univ. Cambridge (1982).
15. Richter, F. M., Nataf, H. C. & Daly, S. F. *J. Fluid Mech.* **129,** 173–192 (1983).
16. Murase, T. & McBirney, A. R. *Geol. Soc. Am. Bull.* **84,** 3563–3592 (1973).
17. Richet, P. & Bottinga, Y. *Geochim. cosmochim. Acta* **44,** 1535–1541 (1980).
18. Bottinga, Y., Richet, P. & Weill, D. F. *Bull. Miner.* **106,** 129–138 (1983).
19. Urbain, G., Bottinga, Y. & Richet P. *Geochim. cosmochim. Acta* **46,** 1061–1072 (1982).
20. Merzkirch, W. *Flow Visualization* (Academic, New York, 1974).
21. Sparrow, E. M., Husar, R. B. & Goldstein, R. J. *J. Fluid. Mech.* **41,** 793–800 (1970).
22. Turner, J. S. *Buoyancy Effects in Fluids* (Cambridge University Press, 1973).
23. Gill, A. E. *J. Fluid Mech.* **26,** 515–536 (1966).
24. Baines, W. D. & Turner, J. S. *J. Fluid Mech.* **37,** 51–80 (1969).
25. Donaldson, C. H. *Miner. Mag.* **41,** 323–336 (1977).
26. Samoylovitch, Y. A. *Geochem. Int.* **16,** 79–84 (1979).
27. Brandeis, G., Jaupart, C. & Allègre, C. J. *J. geophys. Res.* (submitted).

# Isotope composition of sulphate in acid mine drainage as measure of bacterial oxidation

**Bruce E. Taylor & Mark C. Wheeler***

Department of Geology, University of California, Davis, California 95616, USA

**Darrel Kirk Nordstrom**

Water Resources Division, US Geological Survey, Menlo Park, California 94025, USA

**The formation of acid waters by oxidation of pyrite-bearing ore deposits, mine tailing piles, and coal measures is a complex biogeochemical process and is a serious environmental problem. We have studied the oxygen and sulphur isotope geochemistry of sulphides, sulphur, sulphate and water in the field and in experiments to identify sources of oxygen and reaction mechanisms of sulphate formation. Here we report that the oxygen isotope composition of sulphate in acid mine drainage shows a large variation due to differing proportions of atmospheric- and water-derived oxygen from both chemical and bacterially-mediated oxidation. $^{18}O$-enrichment of sulphate results from pyrite oxidation facilitated by *Thiobacillus ferrooxidans* in aerated environments. Oxygen isotope analysis may therefore be useful in monitoring the effectiveness of abatement programmes designed to inhibit bacterial oxidation. Sulphur isotopes show no significant fractionation between pyrite and sulphate, indicating the quantitative insignificance of intermediate oxidation states of sulphur under acid conditions.**

The overall stoichiometry of pyrite oxidation may be described by the reaction: $FeS_2(s)+\frac{15}{4}O_2(aq)+\frac{7}{2}H_2O \rightarrow Fe(OH)_3(s)+2H_2SO_4(aq)$. In order to understand the oxidation kinetics, intermediate steps in this reaction must be considered[1]. The following three reactions have been shown to operate under acid conditions[2–5]:

$$FeS_2(s)+14Fe^{3+}+8H_2O \rightarrow 15Fe^{2+}+SO_4^{2-}+16H^+ \quad (1)$$

$$Fe^{2+}+\tfrac{1}{4}O_2+H^+ \rightarrow Fe^{3+}+\tfrac{1}{2}H_2O \quad (2)$$

$$FeS_2+\tfrac{7}{2}O_2+H_2O \rightarrow Fe^{2+}+2SO_4^{2-}+2H^+ \quad (3)$$

Below a *p*H of 3, reaction (2) is thought to be the rate-limiting step for reaction (1), the principal inorganic oxidation mechanism[3]. *Thiobacillus ferrooxidans* increases the rate of oxidation of ferrous to ferric iron (reaction (2)) by several orders of magnitude in acid environments[4,6,7]. This microbial influence on pyrite oxidation is usually referred to as indirect action, as distinguished from a direct action mechanism in which *T. ferroxidans* or other microbes attach themselves to the pyrite surface[8,9] and directly attack the surface, enzymatically oxidizing sulphide to sulphate, similar to reaction (3)[5].

The roles and sources of oxygen may thus be quite varied. In reaction (1) the sulphate oxygen is derived from the water molecule whereas in reaction (3) it is derived from dissolved

* Present address: US Geological Survey, 345 Middlefield Road, Menlo Park, California 94025, USA.